Springer

KSME

Journal of Mechanical Science and Technology 32 (12) (2018) 5659~5669
www.springerlink.com/content/1738-494x(Print)/1976-3824(Online)
DOI 10.1007/s12206-018-1113-9

Practical payload assessment of a prototype blade for agricultural unmanned rotorcraft †

Y. M. Koo[1,*], J. G. Hong[1], B. A. Haider[2] and C. H. Sohn[2]

[1]*School of Agricultural Civil and Bio-industrial Engineering, Kyungpook National University, Daegu 41566, Korea*
[2]*School of Mechanical Engineering, Kyungpook National University, Daegu 41566, Korea*

(Manuscript Received November 27, 2017; Revised August 3, 2018; Accepted September 28, 2018)

Abstract

Unmanned rotorcraft represents a new paradigm in agricultural activities. Rotor-blade design to improve lift performance was necessitated because payload-mounted flights suffer from a lack of lift. A prototype of rotor blade, comprising the V2008B airfoil, was assessed on an agricultural rotorcraft. The lift corresponding to the collective pitch angle (CPA) and rotor speed was measured on field and compared with a base-line blade. Measurements demonstrated that the prototype blade could sustain a maximum payload of 589 N, resulting in a total lift of 1256 N. Thus, an increase of 10.5 % in total lift was accomplished, compared with a base-line of 1137 N. Simulation also indicated that total lift equals 1269 N at CPA = 10°, approximately 1.0 % greater than the experimental lift. However, a practical spray payload would be reduced due to the ground effect and uncertainty, existing during an anchored field experiment. The ground effect from the experimental operation close to the ground would reduce 10 % of the total lift, resulting in 1138 N for hovering. Furthermore, uncertainty existed in stick control inputs and local wind conditions, resulting in fluctuations of rotor speed and payload. The standard deviation of net lift was ±45.33 N; therefore, the minimum net lift of the low envelope assessed from the uncertainty analysis would be 426 N.

Keywords: Rotor blade; Field lift test; Uncertainty; Ground effect; Agricultural unmanned rotorcraft

1. Introduction

Pesticide spraying on agricultural crops in Korea is labor-intensive and inefficient and is thus often avoided. It is, therefore, necessary to establish a pesticide application system that facilitates efficient and stable agricultural production along with a safe working environment for farmers. With the ageing of rural manpower in Korea, mechanization and automation of agricultural technology have become increasingly important. Therefore, research activities focusing on development of pesticide application techniques for farmers have gained increased attention in recent years [1].

Agricultural unmanned aerial vehicles are becoming increasingly popular for use in pesticide application. The aerial pesticide application technology offers great superiority in terms of timely application, small-scale precision farming, increased field capacity, and reduced reliance on human labor.

According to Koo et al. [2], agricultural helicopters tend to maintain aerodynamic characteristics close to those observed in hovering flight because they fly at slow speeds of the order of 15–25 km/h. As agricultural helicopters are small and operate at low velocities, their blade-airfoil sections, contrary to those of commuter helicopters (4×10^6– 10×10^6), demonstrate low Reynolds number (1×10^6– 3×10^6) characteristics [3, 4].

Considering the characteristics of hovering flight, the power unit of the helicopter must provide sufficient power to overcome the dead weight as well as sustain a payload. However, during summer and/or in highland areas, payload-mounted flights suffer from a lack of lift that cannot be solved by simply increasing the engine power. This is because the increase of engine power is accompanied by an increase in its own dead weight [5]. This calls for an improvement in rotor-blade airfoil design.

A major factor influencing the performance of helicopters is the rotor-blade design, which, in turn, depends on the type of airfoil section that influences its lift and drag characteristics. While designing a rotor blade, it is important to maintain good hovering and forward flight performances along with high power efficiency [6].

Won et al. [7] performed, thus, a wind-tunnel experiment on a 3D-printed blade, the airfoils of which were to be used in the design of agricultural unmanned helicopter rotors. In their experiment, a blade section was installed on an adapter placed at the exit of the wind tunnel, and the lift and drag forces were measured using multi-axis load cells. Furthermore, aerody-

*Corresponding author. Tel.: +82 53 950 5788, Fax.: +82 53 950 6780
E-mail address: ymkoo@knu.ac.kr
† Recommended by Associate Editor Seongwon Kang

namic characteristics of the concerned blade section were predicted using computational fluid dynamics (CFD) simulations and the CFD model was verified by comparing the simulation results with those obtained from the wind-tunnel experiment. The V2008B airfoil demonstrated stable lift characteristics at angles within the range of 7–9° and the end blade consumed a power of approximately 14–15 kW. The induced power accounted for more than 79 % of the total power consumed while the profile power accounted for approximately 21 %.

Analysis of existing rotors and design of new rotors are considered to be areas of keen interest in the helicopter-rotor design. Existing rotors can be analyzed through wind-tunnel experiments or by performing blade-lift tests on a rotating tower [3]. However, analysis for performance estimation in actual situations, such as hovering and forward maneuvers, are difficult to perform. Helicopter performance can, therefore, be predicted through demonstration experiments and verification of CFD simulations [8].

The aerodynamic design of the rotor blade was evaluated for an agricultural unmanned helicopter using the multiple reference frame based on Navier–Stokes analysis. Three different blade designs (V1505A, V2008B and V1215C) were investigated by varying the airfoil shape and twist angle. The performance parameters (lift, torque, power, and figure of merit) were analyzed at various collective pitch angles (CPA) in the hovering condition for a constant rotational speed of Re = 1.3×10^6 at the tip. Both the untwisted and twisted blades with highly cambered airfoil section (V2008B) were aerodynamically more efficient and had the capacity to produce large thrust when compared to a base-line blade with relatively thick and less camber airfoil section (V1505A) [9].

Abhiram et al. [10] conducted a robust design employing the Taguchi method on type-I unmanned rotorcraft, and resulting an 11.28 % reduction in power required to hover when compared with a baseline helicopter (R20, Yamaha Motors Ltd, Co., Japan). In the optimization, selected four parameters were rotor radius, tip chord related with blade taper, linear twist of the blade and the rotor speed. Even though there is significant reduction in hover power, the figure of merit (FM) remains almost the same because of the difference in the disk loading factor.

Haider et al. [11] conducted additional research on the V2008B airfoil and reported an optimum airfoil design via Design Xpert® by employing response surface methodology (RSM) to improve the hovering flight efficiency of the agricultural helicopters. Solutions to Reynolds-averaged Navier–Stokes (RANS) equations and multiple reference frames (MRF) were used in the analysis. Their proposed optimal rotor blade demonstrated a 12 % improvement in hovering flight efficiency when a total of 15 design points were set by combining several variables. In their study, blade grip and tip angles of attack (AoA) were used to determine the twist angle and airfoil chord length using objective functions for rotor torque, thrust, power, and figure of merit.

Practical rotor-blade performance, in general, is evaluated through lift tests. For example, Caradonna and Tung [12] conducted an experiment to determine the lift characteristics of and pressure distribution around the NACA 0012 airfoil, which is used as a reference for verifying airfoil designs and aerodynamic-analysis models. Winkelmann et al. [13] conducted wind-tunnel experiments on the leading-edge stall phenomenon of variable wings using the NACA 0015 and NACA 64A211 airfoils operating at low Reynolds numbers. Koo et al. [14] measured the lift force generated by a helicopter rotor comprising a test blade (SW04) by using a load cell to investigate the performance of an agricultural unmanned helicopter rotor blade.

The downwash that occurs when a helicopter flies close to the ground influences an interaction with the ground and affects the flow near the rotor disc. The downwash, in particular, is reflected off the ground and serves to increase the lift generated by the rotor, thereby effectively decreasing the power required for a given lift [15]. Experiments performed in extant studies to investigate the impact of ground effect in hovering flight report an increase in lift of the order of 10–15 % [16-18]. Tanabe et al. [19] compared the results of CFD simulations using overlapping grids with the Cheeseman–Bennett line. Their results indicate that the lift and, thus, required power decrease by approximately 12 % as the ratio of the rotor radius to height from the ground was decreased.

Uncertainty exists in the field maneuvers such as angular velocity and radius of main rotor, chord and taper of main blade, local environment conditions, system control inputs and data measurement. The propagation of these parameters extends into the performance of helicopter such as lift, FM, power requirement and induced velocity. Siva et al. [20] presented the effect of uncertainty on performance predictions of a helicopter using Monte Carlo simulations (MCS) and the first-order reliability methods (FORM). The power coefficient for hover case showed a large scatter in the predictions with a CV of 8.33 % and ranging from -30 % to 45 % from the baseline.

The uncertainty effect is presented in the form of percent deviation and/or the coefficient of variance (CV) from the baseline. The uncertainty effect on power requirements of linear twisted blade showed a CV of 5.03 % and increase of power requirement by about 5 to 10 % [21]. Experiments need to reveal statistical deviation for the uncertainty effect.

Concluding a series of previous studies [7, 9, 11], a prototype of rotor blade was manufactured and assessed via field measurement. As a consequent process, therefore, this study aims to investigate the lifting characteristics of the rotor blade, comprising and named after the V2008B airfoil using a free-style lift measuring system equipped on an agricultural helicopter (AgroHeli-4G). Then, the performance of V2008B blade was compared with that of a base-line blade comprising V1505A airfoil. Test results of the prototype were practically determined with those obtained via CFD simulations reflecting the ground effect and uncertainty of field maneuver in order to assess a lower envelope of net lift for the designed rotor.

Table 1. Geometrical characteristics of the prototype V2008 airfoil and base-line (V1505A) airfoil.

Parameters	V2008B	Baseline
Maximum thickness	0.131	0.179
Maximum camber	0.027	0.020
Maximum thickness location	0.328	0.301
Maximum camber location	0.334	0.171
Leading edge radius	0.014	0.028

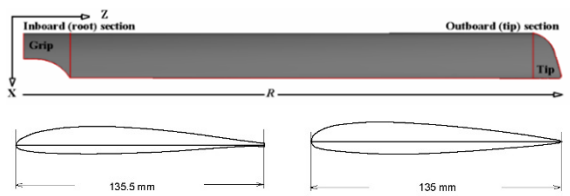

(a) Prototype (b) Base line

Fig. 1. Geometry model of the rotor blade designed and named after (a) V2008B airfoil; (b) a base-line (V1505A) airfoil.

2. Material and methods

2.1 Blade geometric characteristics

Fig. 1 depicts a 3D model of the rotor blade comprising and named after V2008B airfoil and base-line, investigated by Won et al. [7] and Haider et al. [9, 11]. A twisted blade with V2008B airfoil section is aerodynamically more efficient and have the capacity to produce better lift when compared to blades with relatively thick and less cambered base-line, i.e. V1505A. The chord length of the prototype airfoil is 135.5 mm and the length of the rotor blade is 1380 mm. The airfoil maximum thickness and camber are expressed as fractions of the chord length (Table 1). The prototype airfoil has a sharp, drooped nose with a large camber, thereby exhibiting the characteristics of leading-edge stall, which occurs in thin airfoils having a drooped nose and large camber. On account of the effect of increased camber near the leading edge, the laminar separation layer rapidly attaches to the airfoil surface, thereby creating a transition zone. This facilitates the achievement of high lift and low drag coefficients at low angles of attack and high Reynolds numbers [3]. The rotor radius (R) from the center of rotation of the rotor blade to the blade tip was 1580 mm, and the twist angle was −5° (Table 2).

2.2 Experimental lift measurement

As shown in Fig. 2, a freestyle payload-measuring system was applied to the agricultural helicopter (AgroHeli-4G) developed by the Kyungpook National University, Daegu, Korea, and the total dead weight, including the load-cell system, measured 667 N (68 kg_f) (Table 2).

The objective of the freestyle payload experiment was to assess the lift force considering the trim condition of the helicopter prior to a practical payload flight. The load cell (L2350/L2, Futek, Irvine, CA, US) was attached to the bottom of the helicopter, which was equipped with a landing skid, and anchored to the ground. The load cell was subjected to a tensile force when the dead weight was overcome by lift generated by the rotor blades; in this case, we say that a payload is exhibited. The rotational speed of the main rotor was measured in real time by an encoder (S40-6-0050ZV, Metronix Co., Korea) mounted on the tail shaft by considering a suitable gear ratio with respect to the tail rotor (Fig. 3). Signals received from the load cell and encoder were displayed on digital displays (L20010WM1, Laurel Elec. Inc., Costa Mesa, CA, US), to facilitate real-time monitoring during the experiment, and stored at an interval of 100 ms into a data logger (CR850, Campbell Scientific Inc., Logan, UT, US). A wireless data system measured the collective pitch angle (CPA) of the blade grip in real time, as described in Sec. 2.3 [22].

Table 2. Specifications of the helicopter and rotor blade V2008B used in the freestyle payload-measuring test.

Parameters	Specification, unit
Engine power	24.5 kW (32 PS)
Dead weight	667 N (68 kg_f)
Fuselage length	3810 mm
Nominal rotating speed	1000 rpm
Number of blades	2
Rotor diameter	3160 mm
Twist angle	−5°
Blade aspect ratio	10.0
Rotor solidity	0.0569
Re @ tip	1.54×10^6
Mach @ tip	0.487

Fig. 2. Freestyle payload measuring system using an agricultural helicopter (AgroHeli-4G) of university's own design.

2.3 Collective grip pitch angle

To investigate lifting characteristics of the agricultural helicopter, real-time measurements of the stick input signals to the transmitter were required. These data enable the lift corresponding to the grip CPA of the blade to be analyzed in terms

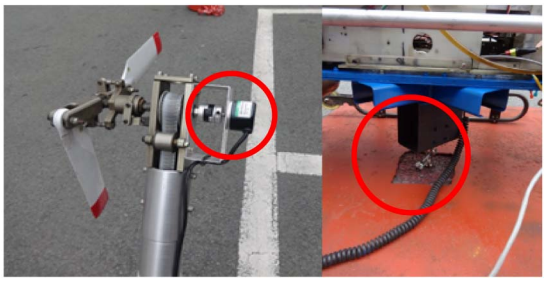

Fig. 3. Payload-measuring system using an encoder and load cell.

(a)

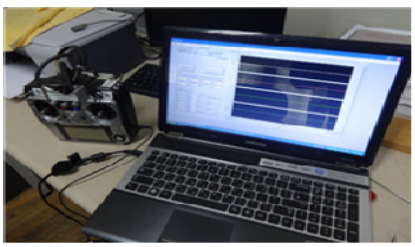

(b)

Fig. 4. (a) A commercial transmitter for controlling the helicopter; (b) stick-position receiver for monitoring and saving the collective pitch angle (CPA) with the freestyle payload-measuring system data.

of controller manipulation. The field lift test was conducted using the stick position transmitter developed by Park et al. [23], and the grip CPA was determined from the stick position of the controller.

Fig. 4(a) depicts a commercial RC controller (T10CHG, Futaba, Japan) equipped with a position transmitter for the sticks and a toggle switch. In order to read the collective pitch (CP) stick input signal from the controller, the signal was wirelessly transmitted via a Bluetooth module (FB755A, Firmtech Co., Ltd., Korea). Fig. 4(b) shows the stick position monitoring program of the controller, which was created using LabVIEW® (V2009, NI, Austin, TX, US) and provides a graphical display of the stick position that can be observed in real time. The data records were separated for each channel and converted into a percentage based on the center position of the stick; this information was then stored at every 20 ms in the form of raw CP data.

Eq. (1) is a third-order regression polynomial that predicts values of the rotor-grip CPA from stick position shown in Fig. 5. The CP stick position transmit (TR) raw data determines the grip angle corresponding to the curve, which has been adjusted to facilitate fine-grained manipulations by flattening the slope of the CPA center, where the helicopter reacts most sensitively. Mechanical backlash of the servomotor controlling the rotor grip caused a hysteresis phenomenon to occur in the signals when the stick was raised and lowered. However, the deviation was small, and the regression polynomial was obtained by integrating the upward and downward data. The following equation was then used to evaluate real-time CPA.

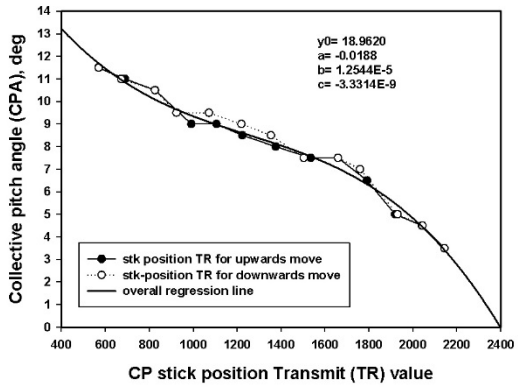

Fig. 5. Regression curve fit of CPA and TR raw data corresponding to the CP stick position.

$$y = 18.9620 - 0.0188x + 1.2544 \times 10^{-5} x^2 - 3.3314 \times 10^{-9} x^3 \quad (1)$$

where y and x respectively represent the grip CPA and TR raw data of the CP stick position.

Any change in CP stick position causes a corresponding change in the grip angle of the main rotor, thereby controlling the lift of the rotor. CPA is manipulated by the stick position of the controller and is interlocked with the throttle used to adjust the engine rotational speed [4]. To predict rotor performance of the helicopter, the rotational speed of the rotor in the CPA range of 7–10.5° was coupled with the engine speed in the range of 650–1050 rpm. The CPA and rotor speed in the field experiment, therefore, could be reflected in the CFD simulations.

2.4 Uncertainty in the field test

In the experiment, the effects of structural and aerodynamic uncertainty on helicopter performance present themselves. The parameters of uncertainty in the stick command and local weather conditions may propagate the fluctuations of rotating speed, then extend to lift performance and power. The degree of uncertainty is revealed in the form of deviations from means, such as standard deviation (SD), CV or percentage deviation. Results of the uncertainty analysis show the confidence range of lift performance.

Local weather condition such as wind direction & velocity and temperature was monitored during the payload tests using a weather station (21X, Campbell Scientific Co., Logan, UT, USA) located near the test site, as describe Sec. 2.2. The de-

viation of the weather condition was determined for the aleatory uncertainty analysis.

The control transmitter shown in Fig. 4 is equipped with two control sticks commanding four functions of pitch, yaw, roll and collective pitch(CP) [23]. As described in Sec. 3.2, the CP stick plays a major role to exert the lift force; however, the rest of the sticks may also affect the uncertainty of performance. The deviations of the stick positions were analyzed from their base-lines. CPA is manipulated by the stick position of the control transmitter and is interlocked with the throttle used to adjust the rotating speed [4]; thus, the time range of analysis was 10 s concerning the uncertain fluctuation during payload demonstration.

Effects of uncertainty due to the stick command and weather condition to the payload and rotating speed of main rotor are considered using the deviations of aerodynamic performance. The range of deviation indicates the design the envelope of performance and requirements. Effect of uncertainty would be determined by comparing the levels of the uncertainty parameters with those in the performance of agricultural helicopter.

2.5 Simulation model

Performance analysis of agricultural unmanned helicopters is an important task for which CFD simulations may be considered as a useful tool, since practical lift measurements through real-time maneuvers are difficult to obtain detailed aerodynamic characteristics such as drag, torque and thrust. The simulation flow field was created by employing a multiple reference frame (MRF) model [9]. The cylindrical flow field surrounding the rotor was set to 20R (where R is the blade radius) in diameter and 10.8 R in height, and incorporated a stationary zone and a moving zone. The moving zone was set to 6R in diameter and 3.3R in height, and placed at a height of 0.4R from the bottom. Flow across the interface of stationary zone between moving zone was uninterrupted. The top surface of the stationary zone was specified with the inlet velocity while the side surfaces were specified with far-field pressure. The bottom surface was simulated as a disc-shaped solid wall (Fig. 6(a)).

The blade was placed at a height of 0.7 R (where R is the blade radius) from the ground, and appropriate wall boundary conditions were applied to simulate the ground effect. As previously described, ground effect refers to aerodynamic interference in the flow field around a rotor resulting from downwash reflection off the ground [17]. In the case of on-field lift measurements obtained in the freestyle experiment, during helicopter operation close to the ground, the predicted lift force may have been slightly increased by the ground effect. In order to simulate these aerodynamic effects, consideration of the ground effect becomes important when implementing near-ground anchored conditions in the simulation model.

Meshes were created using Ansys meshing (Fluent, v16.2, Ansys Co. Inc., Canonsburg, PA, US), and the number of nodes was set to approximately four-millions after performing a grid sensitivity analysis. A high-density mesh tends to increase the accuracy of lift prediction. Therefore, the growth rate of the mesh was set to 1.25, and the region immediately adjacent to the rotor blade was represented by a high-density grid [24]. High-density mesh layers were generated in the area surrounding the rotor surface, as shown in Fig. 6(b), owing to higher density of the flow around the rotor blade. Using the realizable k–ε turbulence model, which is easy to interpret outside the boundary layer on the rotor surface, the simulation was performed in $5< y^{+} < 250$.

A grid independence was examined by generating meshes of three different sizes—coarse mesh (G1: 2262105 nodes), medium mesh (G2: 4427241 nodes), and fine mesh (G3: 6129223 nodes) —for the rotor blade in order to predict the lift and drag on normalized mesh cells and thereby determining how the mesh quality affects CFD simulation results. Grid sensitivity was verified for CPA = 10° at 1000 rpm (Table 3).

Table 3. Mesh sensitivity in terms of grid number for the convergence of forces simulated for the prototype blade at CPA = 10° at 1000 rpm.

Forces	Grid density	Computed (N)	Percent difference (%)
Lift	G1	1272.1	0.236
	G2	1269.1	0.008
	G3	1269.0	
Drag	G1	110.3	0.181
	G2	110.1	0.098
	G3	110.0	

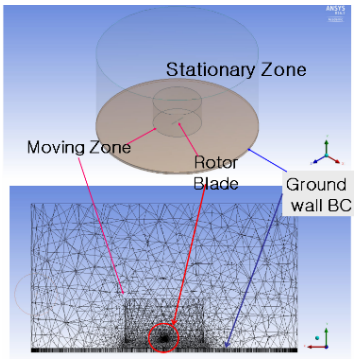

(a)

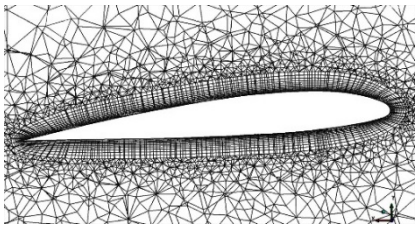

(b)

Fig. 6. (a) MRF mesh structure with wall boundary condition at the bottom of flow field to represent ground effect; (b) mesh generation near airfoil surface.

Based on the sensitivity analysis, percent differences in the case of the medium-grid solution were found remain stable, and there exist negligible differences between the results obtained using the medium and fine grids; the medium grid (about four-millions), therefore, represents a reasonable compromise between accuracy and simulation time required. Hence, the medium grid was used in all simulations performed in this study.

To analyze the performance of the rotor blade, following aerodynamic coefficients are defined. The lift and drag coefficients (C_L and C_D, respectively) are given by Eqs. (2)-(4).

$$C_L = \frac{L}{\rho A(\Omega R)^2} \quad \text{and} \quad C_D = \frac{D}{\rho A(\Omega R)^2} \tag{2}$$

while the torque coefficient (C_T) is

$$C_T = \frac{T}{\rho A(\Omega R)^2 R}. \tag{3}$$

Here, ρ represents ambient-air density, Ω is the rotor speed, R . is the rotor radius, A (= πR^2) is the rotor disc area, L is the lift, and T is the torque. The helicopter efficiency can also be represented by the figure of merit (FM), which is the ratio of the induced power and the available axle power, given by

$$FM = \frac{C_L^{1.5}}{\sqrt{2}\, C_T}. \tag{4}$$

3. Results and discussion

3.1 Field lift measurement

Fig. 7 represents results obtained from field measurements performed during the freestyle lift test. The helicopter lifted the dead weight of 667 N (68 kg_f) and demonstrated the ability to sustain a payload at CPA = 8° (raw data of CP position = 1400). At CPA = 10° (CP position = 900), the helicopter could sustain a payload of 589 N (60 kg_f), thereby generating a total lifting force of 1256 N. This practical operating range of CPA was found to be lying far below the blade stalling angle (approximately 18° [9]). The rotational speed, however, was found to decrease beyond CPA = 10°. The practical value of CPA obtained by the rotor was, therefore, limited by engine power, which was 24.5 kW for the experimental helicopter used in this study.

Fig. 7 shows the on-field test during 30 s; however, the payload exerts for 10 s from taking-off to the demonstration of maximum payload. In the 'payload demo range' the uncertainty analysis is conducted for the stick command and weather condition to the payload and rotating speed of main rotor.

Fig. 8 depicts an improved payload of the prototype blade (V2008B), compared with the base line (V1505A) in terms of

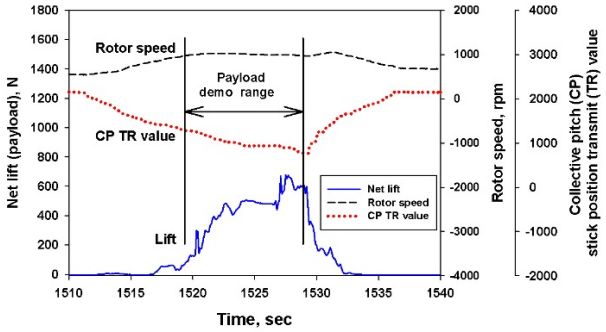

Fig. 7. Field test results of net lift (payload) for the prototype (V2008B) coupled with blade rotating speed and CPA expressed by CP stick position in the demo range of time.

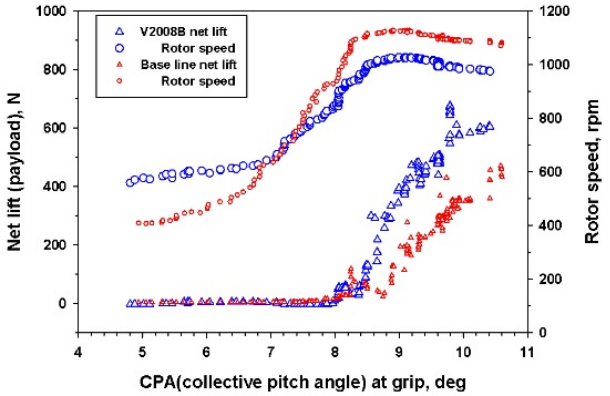

Fig. 8. Demonstrating improved payload of the prototype rotor blade (V2008B) for practical rotor speed and CPA, compared with the baseline blade.

the actual CPA and rotor speed measured during the on-field experiment. At CPA = 8° (at 890 rpm), The lift of the helicopter overcomes its dead weight (667 N) and exhibits payload-sustaining ability for both blades. However, the maximum lift generated by the base line rotor blade at CPA = 10.5° (@ 1100 rpm) was 1137 N (470 N of payload), comparing with the total lift of 1256 N (589 N of payload) at CPA = 10-10.5° (@ 1000 rpm) by the prototype blade (V2008B). Thus, an improvement of 10.5 % in the maximum total lift was achieved by the prototype.

3.2 Uncertainty in payload

Fig. 9 shows the time history of transmitter stick position raw data for pitch, yaw, roll and collective pitch. Then, the collective pitch (CP) position intentionally increased to raise payload and rotor speed. The collective pitch angle (CPA) is also converted from the CP TR value using Eq. (1) of Fig. 5. The uncertainty may be considered during the time of 'payload demon' range. Fig. 10 shows the weather data collected during the time range of payload demonstration, causing the aleatory uncertainty.

Table 4. Uncertainty levels due to the stick input (pitch, roll and yaw) commands and weather (temperature, wind direction and velocity) condition.

Source	Components	Mean	SD	CV	Max	Min
Stick input commands	Pitch TR	1364.8	29.31	2.15	1456	1276
	Roll TR	1280.3	37.45	2.93	1412	1148
	Yaw TR	1508.5	71.23	4.72	1676	1420
Weather conditions	Temp. °C	30.0	0.21	0.71	30.44	29.67
	Wind dir.°	230.9	31.09	13.47	288.4	156.9
	Wind vel. m/s	1.368	0.462	33.78	2.527	0.447

SD: Standard deviation, CV(%): The coefficient of variance

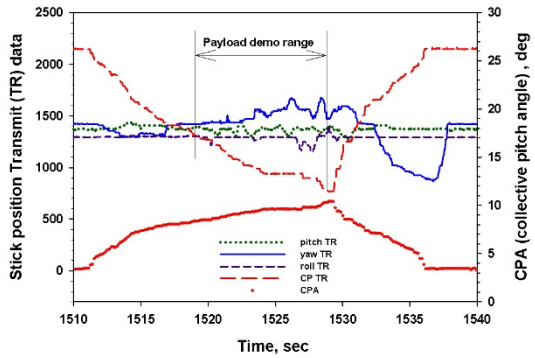

Fig. 9. Stick position TR data of pitch, roll, yaw as well as collective pitch (CP) for the uncertainty analysis during the demo range of time of lift on-field test.

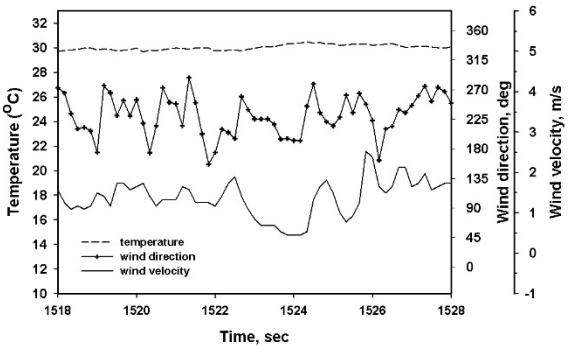

Fig. 10. Weather data of wind velocity & direction and temperature for the uncertainty analysis during the demo range of time of lift on-field test.

Table 4 indicates the levels of uncertainties due to the stick input commands and weather sources. The pitch and roll TRs controlling the attitude of helicopter give the CV about 2-3 % from stick manipulations. However, the yaw TR fluctuates more at the CV of 4-5 % because of the intentional control of yaw stick against anti-torque action in the demo range. The uncertainty consists of 2-3 % due to the stick input and 1-3 % due to the intentional increase of CPA against anti-torque action in the demo range. The uncertainty consists of 2-3 % due to the stick input and 1-3 % due to the intentional increase

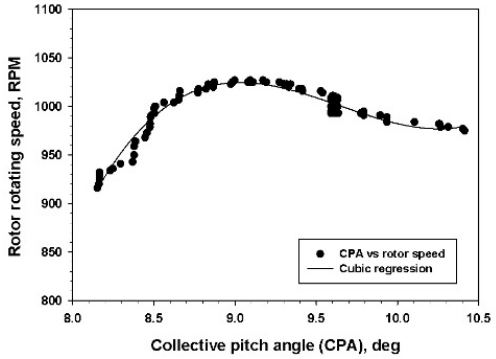

(a)

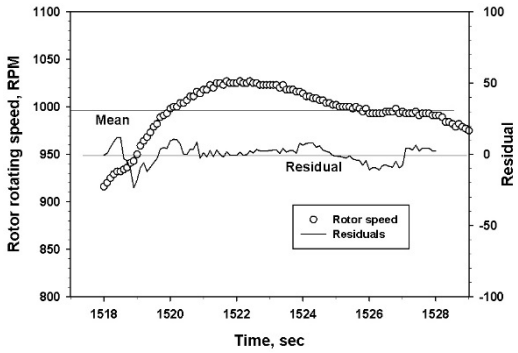

(b)

Fig. 11. (a) Regression of CPA and rotor speed used in determining; (b) the residual deviation in time history due to the uncertainty of CP stick input command.

of CPA.

The uncertainty of temperature is minimal (CV < 1 %), but effects of wind velocity and direction (CV = 14-34 %) to the uncertainty would be significant. The uncertainty of wind condition propagates to lift performance directly, but unlikely to rotor speed.

A third-order polynomial equation (Eq. (5)) was used for the regression of rotating speed to the CPA, presented in Fig. 11(a).

$$y = -35715 + 11284x - 1148.2x^2 + 38.662x^3 \quad (5)$$

where y and x respectively represent the rotating speed (rpm) and the grip CPA (deg).

Figs. 11(a) and (b) show the rotor speeds for the variable of CPA and time history, respectively in the payload demo range. Since the CPA increased to exert payload on purpose, the rotor speed was regressed with the CPA (Eq. (5)). Then the standard error of estimate (σ) and the CV were determined. The CV for the mean of rotor speed in the demo range is 2.73 % (Table 5), which refers to the only effect of stick uncertainty (2-3 %). Therefore, the CV = 0.6 % for the regression is minimal in Fig. 11(b).

A third-order polynomial equation (Eq. (6)) was used for the regression of net lift for the CPA, depicted in Fig. 12(a).

Table 5. The uncertainty propagation to rotor angular speed (rpm) and net lift (N) coupled with the CPA (collective pitch angle), intentionally increased to exert payload.

	Source	Mean	SD (σ)	CV	Max	Min
Input	CPA	9.142	0.539	5.90	9.791	8.152
Propagated to	Rotor speed	997.3	27.22	2.73	1027	986
	Regression	-	(6.397)	0.6	-	-
	Net lift	365.6	187.4	51.25	676.3	28.3
	Regression	-	(45.33)	12.4	-	-

SD : Standard deviation, CV (%): the coefficient of variance,
σ : Standard error of estimate for regression
$= \sqrt{(MSE)} = \sqrt{(SSE)/(n-2)}$

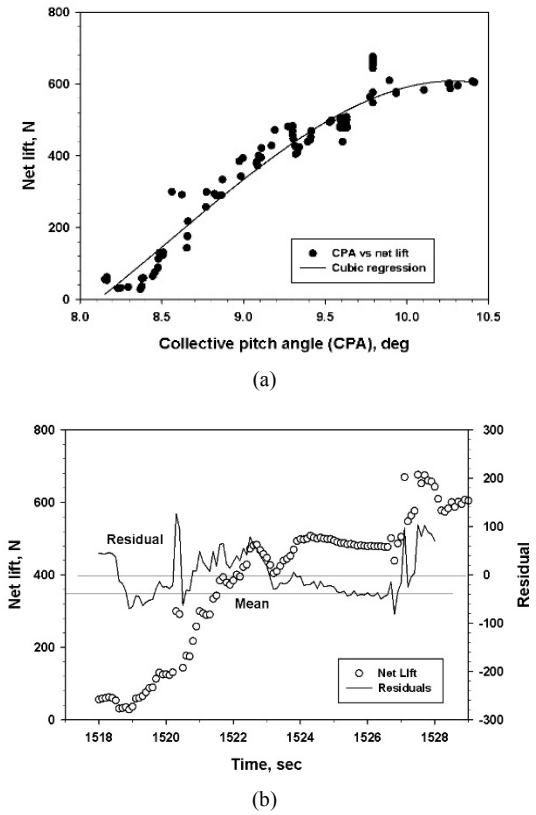

Fig. 12. (a) Regression of net lift and CPA used in determining; (b) the residual deviation in time history due to the uncertainty of CP stick input, rotor speed and weather conditions.

$$y = 23310 - 8895.6x + 1086.1x^2 - 42.368x^3 \quad (6)$$

where y and x respectively represent the net lift (N) and the grip CPA (deg).

Figs. 12(a) and (b) show the net lift for the variable of CPA and time history, respectively in the payload demo range. The CV for the mean of net lift in the demo range is 51.25 % in Table 5, which may refer to the uncertainty effects of stick (2-3 %) and wind velocity (33.78 %) in Table 4. Therefore, the

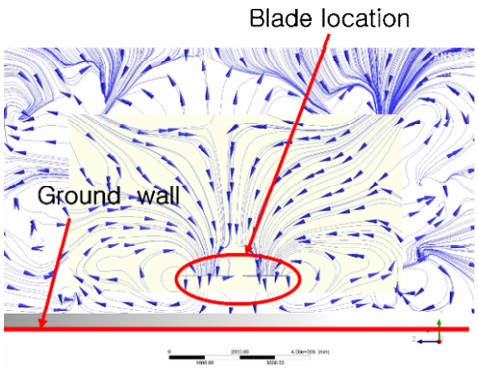

Fig. 13. Velocity streamlines above ground wall.

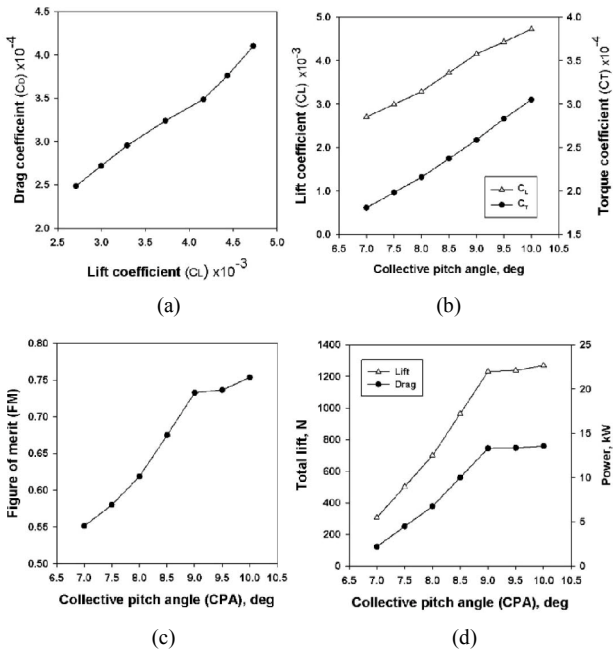

Fig. 14. Aerodynamic performance results of (a) the lift (C_L) vs. drag coefficients (C_D); (b) lift coefficient (C_L); (c) the figure of merit (FM); (d) lift and power to CPA of the prototype blade.

propagated uncertainty (CV = 45-55 %) of net lift for the regression (Eq. (6)) is the summation of the uncertainties from stick input (2-3 %), intentional increasing rotor speed (3-4 %), and wind condition (30-35 %) in the net lift of Fig. 12(b). The uncertainty of CP stick manipulation propagates to the fluctuation of rotor speed, then they propagate consequently to lift performance.

3.3 Performance via simulation

Results from the simulation indicate that the helicopter overcomes the dead weight and is able to sustain a payload at CPA of approximately 8°. When CPA = 10°, the total lift generated and payload sustained by the helicopter along with its drag, torque, and power were estimated to be 1269 N, 602 N

(61.4 kg_f), 110.1 N, 129.4 Nm and 13.6 kW, respectively.

The typical flow pattern in the vicinity of a rotor rotating close to the ground is depicted in Fig. 13. The flow field was seen to be comprised of streamlines entering the blade row and spreading after reflection from the ground, which serves increase of the lift [19].

As shown in Fig. 14(a), the lift (C_L) and drag (C_D) coefficients are seen increase linearly with the slope increasing once CPA exceeds 9°, i.e., when the C_D demonstrates a sharp increase. In Fig. 14(b), the lift (C_L) and torque (C_T) coefficients were found to steadily increase with increase in CPA and ultimately attain values of 4.73×10^{-3} and 3.05×10^{-4}, respectively, at CPA = 10°. When CPA exceeds 9°, the increase in torque coefficient becomes steeper compared to the lift coefficient. This may be attributed to a steeper increase in drag.

Fig. 14(c) depicts the correlation between CPA and FM, wherein FM is seen to increase sharply in the CPA range of 8–9°. This indicates efficient use of power developed by the engine during helicopter take-off. However, once CPA exceeds 9°, the slope of the FM–CPA curve tends to decrease but exhibits FM = 0.73-0.75 showing reasonable efficiency.

As seen in Fig. 14(d), at CPA = 9°, the total lift force generated by the rotor is 1230 N. However, the slope of the lift–CPA curve begins to drop at CPA = 9.5° approximately and remains low until 10°. This is because, as the rotor rotation speed remains constant at about 1000 rpm, the power supply becomes limited, thereby decreasing the total lift generated by the rotor blades. The engine power decreases from about 15.1 kW at CPA = 9° (1050 rpm) to 13.3 kW at CPA = 9.5° (1020 rpm). This may be attributed to limitations imposed by the increase in power required and drag penalty. At CPA = 10° (1000 rpm), a practically optimal operating condition is maintained with an induced power of 13.6 kW. According to Prouty [3], the induced power of the main rotor of a hovering helicopter is about 50–80 % of the total required power. In the proposed study, the induced power was estimated to be 56 % of the total available power (24.5 kW).

3.4 Assessment of practical payload

Prior to extending the simulation model to investigate the aerodynamic characteristics of the concerned rotor blade during hovering and/or forward flights, the lift characteristics of the V2008B airfoil obtained through simulations must be verified in the light of on-field test results. In the field experiment, lift generated by the rotor was measured at certain rotational speeds and CPA values of the rotor blade, which were governed by the throttle settings determined by stick-position signals. At CPA = 8°, the helicopter begins to overcome its dead weight of 667 N and exhibits the ability to sustain a payload, and at CPA = 10°, the payload was 589 N (60 kg_f) i.e., the total lift was 1256 N corresponding to an optimum flying condition. The rotational speed measured during the on-field experiment was 1050 rpm at CPA of 9°. However, as CPA increased to 9.5° and 10°, the rotational speed was found to reduce to 1020 and 1000 rpm, respectively, because of marginal engine power.

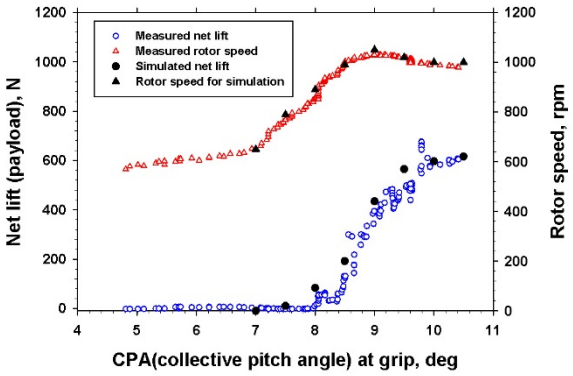

Fig. 15. Practical payload exerted by a pair of the prototype rotor blade comprising airfoil 2008B at various CPAs coupled in the practical rotor speed range via on-field measurement and simulation.

Fig. 15 depicts a comparison of the net payload (excluding the dead weight) sustained by the helicopter as predicted by the simulation and observed during the on-field experiment in terms of the actual CPA and rotational speed measured during the field experiment. At CPA = 10° (at 1000 rpm), the total lift generated by the rotor was 1269 N, comprising an estimated payload of 602 N (61.4 kg_f), which was 1.0 % higher than the experimentally observed total lift. Thus, the reliability of the constructed MRF simulation model could be demonstrated to further analyze the aerodynamic characteristics of the agricultural helicopter through use of a similar simulation model.

Payload of an unmanned helicopter with a pair of the prototype blades, comprising with V2008B airfoil could be assessed by simulation and field measurement. However, a practical payload, exerting during near-hover spraying would be reduced due to the ground effect and uncertainty of field lifting maneuver. The ground effect from the experimental condition of the anchored helicopter operation close to the ground would reduce 10 % in the total lift [7, 11], thus 1138 N of total lift for hovering. In addition, the uncertainty effect on the standard deviation (SD) of net lift was ±45.33 N, shown in Table 5. Therefore, the minimum net lift of the low envelope, assessed from the simulation and uncertainty analysis would be 426 N.

4. Conclusions

Concluding a series of blade studies for an unmanned agricultural helicopter [7, 9, 11], a prototype was designed and should be proven via field measurement. As a consequent process; therefore, this study was conducted to assess the lifting characteristics of the rotor blade, comprising and named after the V2008B airfoil using a freestyle lift measuring system equipped on an agricultural helicopter (AgroHeli-4G).

The maximum lift generated by the base-line rotor blade at CPA = 10.5° (@ 1100 rpm) was 1137 N (470 N of payload), comparing with the total lift of 1256 N (589 N of payload) at

CPA = 10-10.5° (@ 1000 rpm) by the prototype blade (V2008B). Thus, an improvement of 10.5 % in the maximum total lift was achieved by the prototype.

The CFD simulations performed using the MRF technique estimated the helicopter to exhibit payload-sustaining ability. The results confirmed the applicability of the simulation model for the analysis of spraying operations of agricultural helicopters. Uncertainty existed in the field experiments. The uncertainty (CV = 45-55 %) of net lift is the summation of the uncertainties from stick input (2-3 %), intentional increasing rotor speed (3-4 %), and wind condition (30-35 %).

The practical payload, exerting during near-hover spraying would be reduced due to the ground effect and uncertainty of lifting maneuver. The ground effect from the experimental condition of the anchored helicopter operation close to the ground would reduce 10 % in the total lift, thus 1138 N of total lift for hovering. In addition, the uncertainty effect on the standard deviation of net lift was ±45.33 N. Therefore, the minimum net lift of the lower envelope, assessed from the simulation and uncertainty analysis would be 426 N, twice enough to lift a target payload of 196 N (20 kg_f). Thus, an improvement of 37.1 % in the net lift was achieved by the prototype from the base-line (310 N).

Acknowledgments

This work is supported by the National Research Foundation of Korea (NRF) funded by the Ministry of Science, ICT & Future Planning (Grant No. 2015R1A2A2A 01002328).

References

[1] Y. M. Koo, C. S. Lee, T. S. Seok, S. K. Shin, T. G. Kang, S. H. Kim and T. Y. Choi, Aerial application using a small RF controlled helicopter (I) - status and cost analysis, *Journal of Biosystems Engineering*, 31 (2) (2006) 95-101, https://doi.org/10.5307/JBE.2006.31.2.095.

[2] Y. M. Koo, Performance comparison of two airfoil rotor designs for an agricultural unmanned helicopter, *Journal of Biosystems Engineering,* 37 (1) (2012) 1-10, https://doi.org/10.5307/JBE.2012.37.1.001.

[3] R. W. Prouty, *Helicopter performance, stability, and control*, Kreiger Pub., Malabar, FL, USA (2002).

[4] J. G. Leishman, *Principles of helicopter aerodynamics*, Cambridge University Press, N.Y., USA (2002).

[5] Y. M. Koo, Development of a pilot friendly control system with a roll-balancing unmanned agricultural helicopter, *MAFF Research Report. 11-1541000-00863-01* (2011).

[6] C. B. Park, *Helicopter aerodynamics,* R. W. Prouty (Ed.), Kyngmoon Publishing Co., Seoul, Korea (1992).

[7] Y. S. Won, B. A. Haider, C. H. Sohn and Y. M. Koo, Aerodynamic performance evaluation of basic airfoils for agricultural unmanned helicopter using wind tunnel test and CFD simulation, *Journal of Mechanical Science and Technology*, 31 (12) (2017) 5829-5838, https://doi.org/10.1007/s12206-017-1125-x.

[8] P. Doerffer and O. Szulc, Numerical simulation of model helicopter rotor in hover, *Task Quarterly, Institute of Fluid-flow Machinery PAS,* 12 (3) (2008) 227-236.

[9] B. A. Haider, C. H. Sohn, Y. S. Won and Y. M. Koo, Aerodynamically efficient rotor design for hovering agricultural unmanned helicopter, *Journal of Applied Fluid Mechanics,* 10 (5) (2017) 1461-1474, https://doi.org/10.18869/acadpub.jafm.73.242.27541.

[10] D. R. Abhiram, R. Ganguli, D. Harursampath and P. P. Friedmann, Robust design of small unmanned helicopter for hover performance using Taguchi method, Paper No. 2017-0015, *The 55th AIAA Aerospace Sciences Meeting*, Grapevine, TX, USA (2017), https://doi.org/10.2514/6.2017-0015.

[11] B. A. Haider, C. H. Shon, Y. S. Won and Y. M. Koo, Aerodynamic performance optimization for the rotor design of a hovering agricultural unmanned helicopter, *Journal of Mechanical Science and Technology,* 31 (9) (2017) 4221-4226, https://doi.org/10.1007/s12206-017-0820-y.

[12] F. X. Caradonna and C. Tung, Experimental and analytical studies of a model helicopter rotor in hover, *The Sixth European Rotorcraft and Powered Lift Aircraft Forum,* September 16-19*,* Bristol, England (1980).

[13] A. E. Winkelmann, J. B. Barlow, J. K. Saini, J. D. Anderson Jr. and E. Jones, The effects of leading edge modifications in the post-stall characteristics of wings. *AIAA 18th Aerospace Sciences Meeting;* Jan. 14-16, Pasadena, CA, AIAA-80-0199 (1980).

[14] Y. M. Koo, T. S. Seok, S. K. Shin, C. S. Lee and T. G. Kang, Aerial application using a small RF controlled helicopter (III) - lift test and rotor system, *Journal of Biosystems Engineering*, 31 (3) (2006) 182-187, https: //doi.org/10.5307/JBE.2006. 31.3.182.

[15] S. K. Lee, G. Y. Choi and S. M. Chang, *The foundations of helicopter flight,* S. Newman, Inter-vision publishing Co., Seoul, Korea (2003).

[16] A. Betz, *The ground effect on lifting propellers*, NACA TM 836, 17 (2) (1937) 68-72.

[17] I. C. Cheeseman and W. E. Bennett, The effect of the ground on a helicopter rotor in forward flight, *ARC R.&M. No.3021* (1957).

[18] J. S. Hayden, The effect of the ground on helicopter hovering power required, *The 32th Annual National Forum of the American Helicopter Society*, Washington DC, May 10-12 (1976).

[19] Y. Tanabe, T. Saito, N. Ooyama and K. Hiraoka, Investigation of the downwash induced by rotary wings in ground effect, *International Journal of Aeronautical and Space Sciences*, 10 (1) (2009) 20-29, https://doi.org/10.5139/ijass.2009. 10.1.020.

[20] C. Siva, M. S. Murugan and R. Ganguli, Effect of uncertainty on helicopter performance predictions, *Proc. IMechE, 224(G), Journal of Aerospace Engineering* (2009) 549-562, https://doi.org/10.1243/09544100jaero638.

[21] C. Siva, M. S. Murugan and R. Ganguli, Uncertainty quan-

tification in helicopter performance using Monte Carlo simulation, *Journal of Aircraft*, 48 (5) (2011) 1503-1511, https://doi.org/10.2514/1.c000288.

[22] Y. M. Koo, Y. S. Won, J. G. Hong, B. A. Haider and C. H. Sohn, In-situ measurement of lift and CPA for the rotor performance analysis of an agricultural helicopter, *Proceedings of the KSAM & KSPA 2016 Autumn Conference,* 21 (2) (2016) 72.

[23] H. J. Park, Y. M. Koo, Y. Bae, M. Oh, C. O. Yang and M. H. Song. Flight dynamic identification of a model helicopter using CIFER (I) - flight test for the acquisition of transmitter input data, *Journal of Biosystems Engineering,* 36 (6) (2011) 467-475, https: //doi.org/ 10.5307/JBE.2011.36.6.467.

[24] H. J. Jeong, A study on the aerodynamic analysis of 3-D helicopter rotor in hovering for design, *M.S. Thesis*, Department of Aerospace Engineering, University of Ulsan, Ulsan, Korea (2005).

Young Mo Koo received his M.Sc. in Bio & Agricultural Engineering from Rutgers-The State University of New Jersey, USA. He then received his Ph.D. in Agricultural Engineering from Kansas State University, USA. Dr. Koo is currently a Professor at the Department of Bio-industrial Machinery Engineering at Kyungpook National University, Daegu, South Korea. His research interests are computational fluid dynamics and unmanned aerial application technology using agricultural helicopters.

Jong Geun Hong received his B.Sc. and M.Sc. degrees in Bio-industrial Machinery Engineering from Kyungpook National University Daegu, South Korea in 2016 and 2018, respectively. His research interests include rotor computational fluid dynamics and aerial application of agriculture helicopter.

Basharat Ali Haider received his M.Sc. in Mechanical Engineering from the University of Belgrade, Serbia in 2009. Recently, he has received Ph.D. in Mechanical Engineering from Kyungpook National University, Daegu, South Korea in August 2018. His research interests include computational fluid dynamics, aerodynamic design and optimization, immersed boundary and lattice Boltzmann methods, and fluid-structure interaction.

Chang Hyun Sohn received his M.Sc. in Mechanical Engineering from KAIST in 1985. He then received his Ph.D. in Mechanical Engineering from KAIST in 1991. He worked in ADD for 3 years. He also worked in University of Cambridge as a visiting Assistant Professor in 1996. Dr. Sohn is currently a Professor at the Department of Mechanical Engineering at Kyungpook National University, Daegu, South Korea. His research interests are computational fluid dynamics, particle image velocimetry, flow induced vibration and thermal hydraulics.